ORIGINAL PAPER

Analysis and optimization of lead-free perovskite solar cells: investigating performance and electrical characteristics

A. Mortadi[1] · E. El Hafidi[2] · H. Nasrellah[3] · M. Monkade[1] · R. El Moznine[1]

Abstract

Several studies on solar cells using SCAPS-1D were conducted to investigate their performance, which are typically limited to I–V analysis for DC characterization. Therefore, in the present study, a very wide frequency range from 10^{-2} Hz to 10^{12} Hz was employed to explore diffusion processes and investigate the performance of lead-free Perovskite Solar Cells (PSCs) featuring as a novel heterostructure. These investigations concern the optimization of $MASnI_3$ thickness as an absorber. Additionally, the impact of series (Rs) and shunt (Rsh) resistances is also examined. From the I–V analysis, it was determined that the power efficiency (PCE) could be achieved at a thickness of 0.6 μm. Increasing the series resistance (Rs) led to a significant decrease in the fill factor (FF) and (PCE), whereas the shunt resistance (Rsh) demonstrated a notable improvement in both (FF) and (PCE). Analysis of AC characteristics revealed complex impedance (Z*) and modulus (M*) indicative of main ionic transport, recombination, and diffusion processes crucial for optimization. An appropriate equivalent circuit model was developed and validated through deconvolution and theoretical considerations, yielding parameters such as the time constant for each process. It was observed that ionic conductivity and electronic diffusion play key roles in balancing charge collection and recombination losses. The critical influence of series and shunt resistance on low and high-frequency processes was emphasized, underscoring their significance in solar cell efficiency. A strong correlation was established between the evolution of time constants for each process and power conversion efficiency (PCE).

Keywords Lead free perovskite solar cells · Complex impedance (Z*) and modulus (M*) · Time constants · Power conversion efficiency

Introduction

The production of electricity stands at the forefront of global development, serving as an indispensable catalyst for economic growth in both advanced and emerging economies [1–4]. However, this reliance is not sustainable, as the accelerated pace of energy consumption depletes finite fossil fuel supplies. This depletion poses a significant threat to long-term energy security and environmental sustainability [5]. To address these challenges and meet the escalating demand for energy, a fundamental shift towards renewable energy solutions is imperative. Among these alternatives, solar energy emerges as an exceptionally promising candidate. Solar power harnesses the virtually limitless energy from the sun, and photovoltaic cells, a key technology in solar energy, enable the direct conversion of sunlight into electricity [6, 7]. The advantage of solar energy lies not only in its abundance but also in its environmental friendliness. Unlike fossil fuels, solar energy production produces minimal greenhouse gas emissions, contributing to efforts to mitigate climate change [8]. Moreover, solar technologies continue to advance, making them increasingly cost-effective and accessible. Embracing and expanding the utilization of solar energy holds the potential to not only diversify the global energy mix but also to reduce dependence on finite and environmentally harmful resources. This transition to sustainable energy

✉ A. Mortadi
    mortadi.a@ucd.ac.ma

    R. El Moznine
    elmoznine@yahoo.fr; elmoznine.r@ucd.ac.ma

1   Laboratory Physics of Condensed Matter (LPMC), University Chouaib Doukkali, El-Jadida, Morocco

2   Laboratory of Engineering Science for Energy-ENSA, Chouaib Doukkali University, El-Jadida, Morocco

3   Higher School of Education and Training, University Chouaib Doukkali, El-Jadida, Morocco

sources is critical for ensuring a global economy while addressing the pressing challenges of climate change and resource depletion [9, 10].

Perovskite has emerged as a highly sought-after material in the domain of photovoltaic applications due to its unique light-harvesting properties [11–13]. It represents a distinctive set of optoelectrical characteristics, encompassing adjustable band gaps, a high absorption coefficient, extensive carrier diffusion lengths, and impressive charge carrier mobilities. The initial power conversion efficiency (PCE) for perovskite solar cells (PSC), reported by Kojima et al., was 3.8%. A decade later, Cui et al. achieved a significant and remarkable increase up to 20.8% for methylammonium lead iodide PSC. Recently, new studies have been reported with improved efficiency approaching 25.8% [14, 15]. Despite these advancements in PCE, the current stability challenges of perovskite solar cells pose obstacles to their widespread mass production. A key drawback of lead-based perovskite solar cells lies in the presence of lead, a highly toxic element. The European Union's Restriction of Hazardous Substances directive explicitly prohibits the use of lead in any electronics or electrical equipment. Consequently, researchers are actively exploring alternatives to lead as the metal cation in the perovskite photo-absorber [16–18]. Addressing these challenges is crucial to ensure the development of sustainable and environmentally friendly alternatives in the ever-evolving landscape of photovoltaics [19–21].

In our recent study [22], we introduced a new analytical approach for AC characterization of Perovskite Solar Cells (PSCs) by exploring the combination of complex impedance (Z^*) and modulus (M^*) within the frequency range from 10^{-2} Hz to 10^7 Hz. These studies revealed only two processes, assigned to the contribution of ionic conductivity and recombination within the PSC. Therefore, in the present study, a simulation was carried out using the SCAPS-1D software to investigate a tin-based PSC with the device structure (FTO/ZnO/MASnI$_3$/NiOx/Au). It is well known that absorber thickness is one of the key parameters that can significantly affect the performance of the solar cell. In this case, this structure was analyzed from I-V characteristics at different thicknesses of the active layer (MASnI$_3$). Additionally, complex impedance data were generated over a wide frequency range from 10^{-2} Hz to 10^{12} Hz to investigate ionic transport, recombination, and diffusion processes, which are crucial for optimization. Furthermore, the impact of series resistance (Rs) and shunt resistance (Rsh) was also investigated. The combination of complex impedance (Z^*) and modulus (M^*) provides insightful information into how these parameters could influence the efficiency of the solar cell, and their correlations are established and discussed in this study.

Methodology and device structure

The simulations conducted in this study were carried out using SCAPS-1D (solar cell capacitance simulator), software designed for the numerical analysis of solar cells [23]. This software offers a robust platform for simulating solar cells by allowing the incorporation of up to seven different layers in the cell definition panel, making it highly adaptable for solar cell simulations. Customization of various physical properties, including band gap, electron affinity, and dielectric permittivity, among others, can be achieved for different layers through the layer properties panels, facilitating the creation of specific cell structures.

SCAPS-1D provides users with the capability to define necessary working points in the action panel, supporting the grading of all physical parameters and the specification of properties for both front and back contacts. This flexibility ensures a comprehensive exploration of different configurations.

Moreover, the software allows for performing simulations for both AC and DC electrical analyses and displays their results. In DC simulations, the current–voltage characteristics (I–V) offer direct measurements of critical parameters such as short-circuit current density (Jsc), open-circuit voltage (Voc), fill factor (FF), and power conversion efficiency (PCE). For AC simulations, the software enables the generation of complex impedance (Z^*) data across a frequency range. These simulations can be conducted under various conditions, including different bias voltages and temperatures. Solar illumination can be simulated in both dark and different illuminations.

The proposed PSC structure, depicted in Fig. 1, follows the configuration: FTO/ZnO/MASnI$_3$/NiOx/Au. The FTO layer, situated on a glass substrate, serves as the front transparent contact. The ZnO layer plays a crucial role in determining device performance, as it influences electron transport, a pivotal factor affecting power conversion
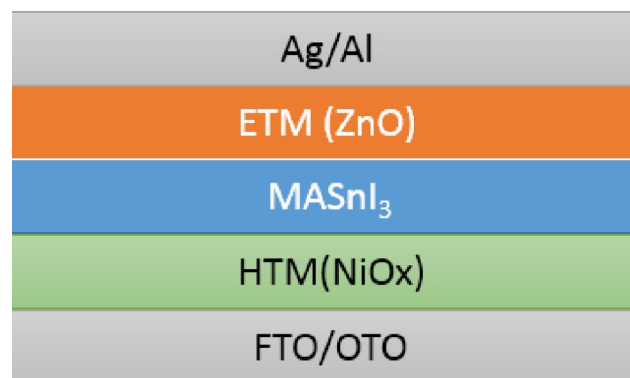

Fig. 1 Schematic structure of perovskite solar cell (PSC)

efficiency (PCE). The MASnI3 perovskite serves as the absorber material, responsible for generating charge carriers through light absorption. Lastly, the NiOx material functions as the hole transport layer (HTL). This detailed structure sets the foundation for the subsequent exploration of parameter variations and their impacts on the efficiency of the solar cell, coupled with an analysis of their correlations with impedance spectroscopy.

The simulation of the FTO/ZnO/MASnI$_3$/NiOx/Au heterostructure solar cell involves the utilization of specific physical parameters, as listed in Table 1.

Additionally, Table 2 provides details regarding the physical properties of defects density. These simulations are conducted under AM 1.5 G (1000 W/m^2) solar illumination and at a temperature of 300 K.

Results and discussion

Current-Voltage Characteristics

Effect of the active layer thickness

Figure 2 illustrates the I–V curve of the proposed Perovskite Solar Cell (PSC) as the perovskite thickness (MASnI$_3$) increases. The figure demonstrates a significant effect on the short-circuit density (Jsc) compared to the open-circuit

Table 1 Physical properties of different layers

Properties	NiOx	MASnI$_3$	ZnO	FtO
Thickness (µm)	80	**0.2–1**	80	0.2
Bandgap (eV)	3.75	1.3	3.2	3.2
Affinity (eV)	2.1	4.2	4.10	4.4
Dielectric permittivity	10.7	10	8.1	9
DOS CB (cm^{-3})	2.8×10^{19}	1×10^{18}	4.5×10^{18}	2.2×10^{18}
DOS VB (cm^{-3})	1.8×10^{19}	1×10^{18}	1×10^{18}	1.8×10^{19}
μ_e (cm^2/Vs)	12	1.6	300	20
μ_h (cm^2/Vs)	25	1.6	1	10
Acceptor concentration (cm^{-3})	1×10^{15}	1×10^{15}	0	0
Donor concentration (cm^3)	0	0	1×10^{19}	1×10^{21}
Defect	1×10^{17}	4.5×10^{16}	1×10^{17}	1×10^{15}

Table 2 Interface parameters of NiOx/MASnI$_3$ and. ZnO/MASnI$_3$

Parameters	NiOx/MASnI$_3$ interface	ZnO/MASnI$_3$ interface
Defects type	Neutral	Neutral
Capture cross-section for electron (cm^2)	1×10^{-19}	1×10^{-19}
Capture cross-section for hole (cm^2)	1×10^{-19}	1×10^{-19}
Energetic distributions	Single	Single
Defects energy level Et	Up the maximum Ev	Up the maximum Ev
Reference for defect energy level Et	0.06	0.06
Total density (integrated over all energies) (cm^{-2})	1×10^{10}	1×10^{10}

Fig. 2 I–V curves for different thickness (**a**) and for 0.2; 0.6; 1 µm (**b**) of perovskite layer
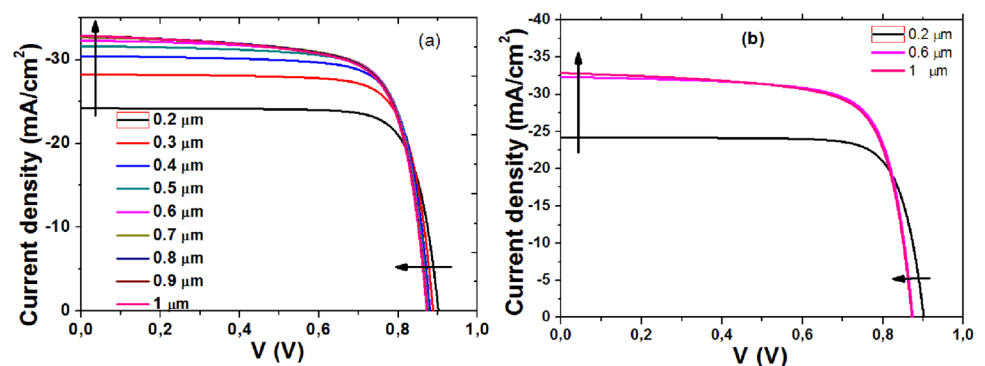
voltage (Voc). This graphical representation serves as a crucial tool for extracting key characteristics that define the solar cell's performance parameters, such as open-circuit voltage (Voc), short-circuit current (Jsc), fill factor (FF%), and efficiency (PCE%). The analysis of these characteristics provides valuable insights into the influence of MASnI3 thickness on the overall behavior and efficiency of the PSC.

The evolutions of Voc, Jsc, FF, and PCE with the thickness of the absorbing material ($MASnI_3$) are shown in Figs. 3a, b. The analysis reveals that the open-circuit voltage (Voc) exhibited a slight decrease as $MASnI_3$ thickness increases, potentially indicating heightened recombination losses or altered charge transport properties. The observed decrease in Voc with increasing thickness is consistent with the findings of studies carried out by Al-Mousoi et al. [21]. The fill factor (FF) also exhibited a rapid decrease up to 0.6 μm, followed by a slower decline, signifying potential equilibrium or saturation effects. In contrast, the short-circuit current (Jsc) displays a significant increase up to 0.6 μm thickness of the absorber perovskite layer, suggesting improved light absorption. The power conversion efficiency (PCE) increased with thickness, reaching a maximum at 0.6 μm, indicating an optimal thickness for MASnI3. Beyond this value, while Jsc remains constant, the decline in FF contributes to an overall reduction in PCE. A similar behavior was observed in our previous study carried out by Mortadi et al. [22], which showed improved optical properties in perovskite layers within a similar thickness range. The consistent Jsc beyond this optimal thickness, coupled with

the decline in FF, aligns with observations made by Rahman et al. [23], reinforcing the importance of the approach for thickness selection.

It is found that the Voc and FF decrease with increasing thickness due to the increase in series resistance. As more absorber layer results in more light absorption, Jsc increases with the thickness of the perovskite layer. Regarding the power conversion efficiency (PCE), it appears that there is a certain absorber thickness (0.6 μm) where the efficiency reaches a maximum, after which it decreases slightly with further thickness increase.

## Impact of the series and shunt resistance (R_s and R_{sh})

The performance of solar cells is substantially governed by the influential characteristics of series resistance (Rs) and shunt resistance (Rsh). Numerous studies [24–26] emphasize the major impact of Rs and Rsh on the efficiency of solar cells. Therefore, the efficiency of the solar cell was evaluated at the optimum value of perovskite thickness (0.6 μm) corresponding to the high efficiency for the Rs value within the range from 0 up to 10 Ω·cm². As depicted in Fig. 4a, b, the increase in Rs values resulted in a significant reduction in both fill factor (FF) and power conversion efficiency (PCE). The observed reduction is consistent with the findings reported in the study [24] conducted for a comprehensive analysis of series resistance effects on solar cell performance. This decline was attributed to the emergence of leakage currents, while the open-circuit voltage

Fig. 3 **a**, **b** Effect of perovskite layer thickness on Voc, Jsc, FF%, and PCE%
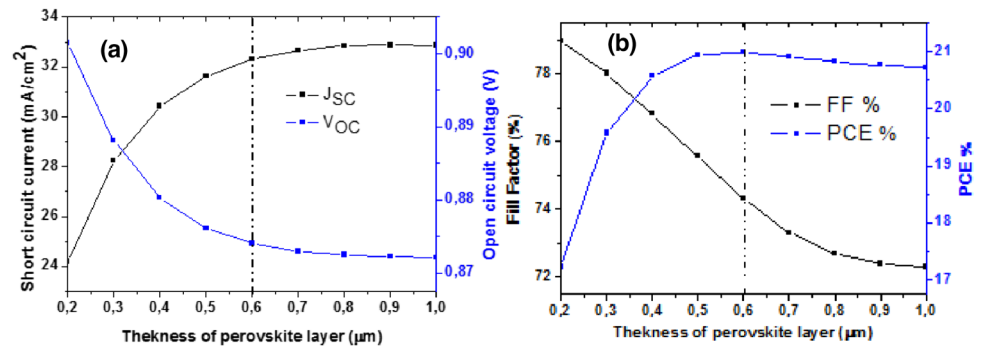
Fig. 4 **a**, **b** Effect of Rs on the V_{OC}, J_{SC}, FF and PCE
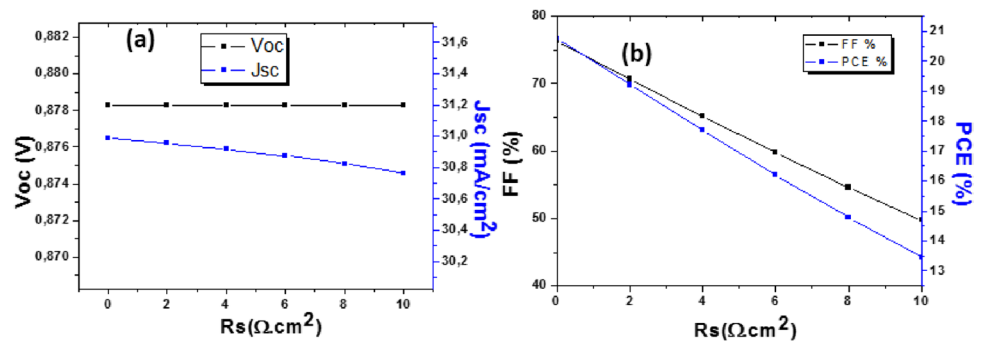
(Voc) showed little change and the short-circuit current (Jsc) exhibited a significant decrease as the value of Rs increases.

The findings highlight the critical role played by Rs in modulating the operational efficiency of solar cells, indicating the intricate interplay between resistance parameters and overall cell performance.

The efficiency of the solar cell was also evaluated at the optimum value (0.6 μm) of perovskite thickness corresponding to the high efficiency for the Rsh value within the range from 200 up to 10^6 $\Omega\cdot cm^2$, as illustrated in Fig. 5a, b.

Conversely to the impact of Rs, it can be seen from Fig. 5a that the short-circuit current (Jsc) showed almost no change. In contrast, the most substantially impacted parameter is the open-circuit voltage (Voc), which exhibited a significant increase as the value of Rsh increased from 200 up to 1000 $\Omega\cdot cm^2$; then it seems to reach almost a plateau above this value. This behavior results in an increase in the FF value and consequently enhances the overall PCE, as observed from Fig. 5b. This result corresponds with the crucial role of shunt resistance in mitigating power losses within the solar cell and emphasizes its potential for optimizing cell performance [25, 26]. Therefore, this result could indicate that the Rsh value within the range from 10^4 up to 10^6 $\Omega\cdot cm^2$ is more appropriate to achieve high and stable efficiency of this structure for the solar cell.

Complex impedance (Z*) and modulus (M*)

The significance of understanding the behavior of organic–inorganic materials in perovskite solar cells (PSCs) has been highlighted in previous research [27, 28]. Unlike conventional inorganic materials, these organic–inorganic hybrids exhibit mixed electronic-ionic conductivity, adding complexity to the comprehension of device mechanisms. The coexistence of electronic and ionic conductivities often complicates the elucidation of operational mechanisms in PSCs. Therefore, gaining a comprehensive understanding of ionic movement, ion/defect migration, and their impact on PSC operational mechanisms is crucial for achieving stability and high performance. To tackle this challenge, impedance spectroscopy (IS), a widely employed technique capable of investigating these processes across various time scales, is utilized. Therefore, in the following section, the effects of perovskite layer thickness, series resistance (Rs), and shunt resistance (Rsh) on PSC performance are investigated through the combination of complex impedance (Z*) and modulus (M*).

Analysis of the complex impedance (Z*) at different perovskite thicknesses

Figure 6a shows the Nyquist plot, presenting the imaginary part (Z″) versus the real part (Z′) of the complex impedance (Z*) at different perovskite layer thicknesses. It can be seen that each curve shows only one semicircle. As the perovskite layer thickness increases, there is a discernible reduction in the diameter of these semicircles. This behavior is indicative of changes in the charge transport properties within the perovskite layer, implying enhanced charge carrier mobility or reduced recombination rates with thicker perovskite layers. This observation is crucial in understanding the impact of perovskite layer thickness on the impedance characteristics and, by extension, on the charge transport dynamics within the PSCs.

Figure 6b displays the imaginary part (Z″) as a function of frequency at different perovskite layer thicknesses. A distinct relaxation process for each thickness is evident. This process is indicative of the time-dependent behavior of charge carriers within the perovskite layer. The maximum shifts towards higher frequencies, and its magnitude decreases as the thickness of the perovskite layer increases. The observed shift is consistent with findings by Mortadi et al. [22]. In this investigation, the frequency-dependent behavior of charge carriers within the perovskite layer exhibited similar trends, attributing these shifts to variations in charge carrier mobility and recombination dynamics.

Simultaneously, Fig. 6(c), depicting the real part (Z′) as a function of frequency, reveals three distinct regions marked by changes in slope. Each region corresponds to a different regime of charge transport or relaxation dynamics within the PSC. These changes in slope may suggest transitions between different charge carrier transport mechanisms or

Fig. 5 **a**, **b** Effect of R_{sh} on the V_{OC}, J_{SC}, FF and PCE
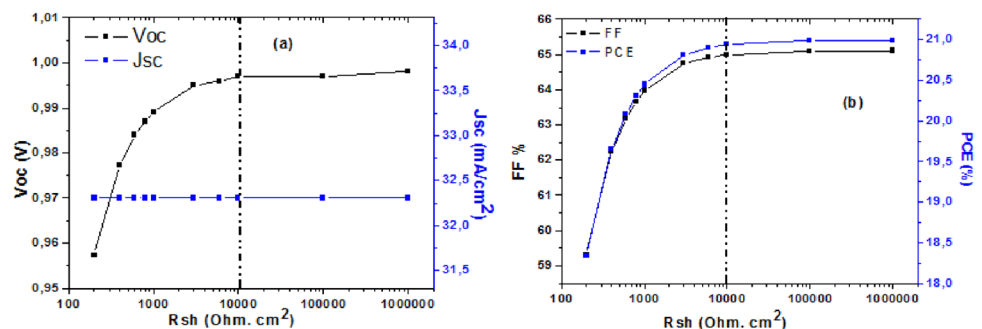
Fig. 6 Impedance spectra **a** Nyquist plot and **b–d** bode plots of solar cell perovskite at different thicknesses of the perovskite layer
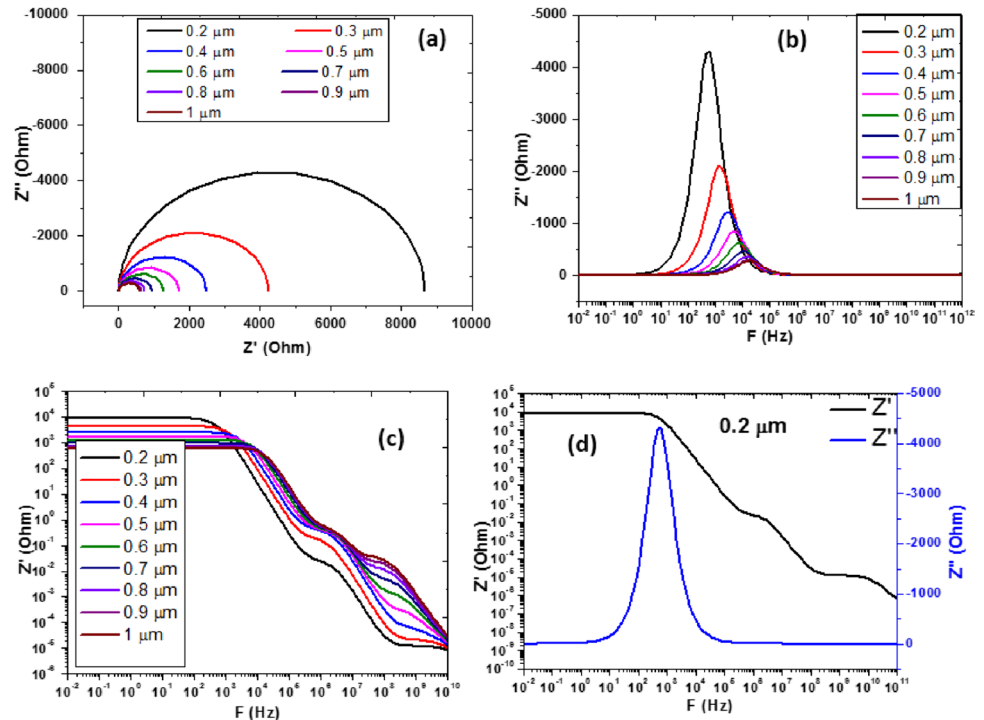
relaxation processes. Therefore, understanding these distinct regions provides valuable insights into the nature of charge transport within the perovskite layer and is essential for optimizing PSC performance, as shown in Fig. 6d as an example graph to illustrate this main change in slope in the curve of (Z′) versus frequency for (0.2 μm).

The comprehensive understanding of these distinct regions, as emphasized in the study, needs further support to investigate these variations in impedance response that are indicative of different processes within the perovskite layer, influencing charge transport and recombination dynamics [29]. For this reason, we explore the complex modulus (M*) based on our previous study [22], where it was very useful in the identification of other processes that could not be observed from the complex impedance (Z*) spectra. The modulus function is a valuable tool in distinguishing

intricate processes within impedance spectroscopy. Its primary significance lies in providing a quantitative analysis, facilitating a nuanced understanding of charge transport dynamics.

Analysis of the complex modulus (M*) at different perovskite thicknesses

Figure 7a, b shows the evolution of the modulus (M*) spectra in Nyquist plot and Bode plots of the solar cell perovskite at different thicknesses of the perovskite layer. From Fig. 7a, three semicircles can be seen, where the diameter of the first seems to be larger than the others. As the perovskite layer thickness increases, the semicircles exhibit a proportional enlargement in their diameters. Specifically, the increases in diameters of these semicircles offer valuable insights into the

Fig. 7 Modulus spectra **a** Nyquist plot and **b** bode plots of solar cell perovskite at different thicknesses of the perovskite layer
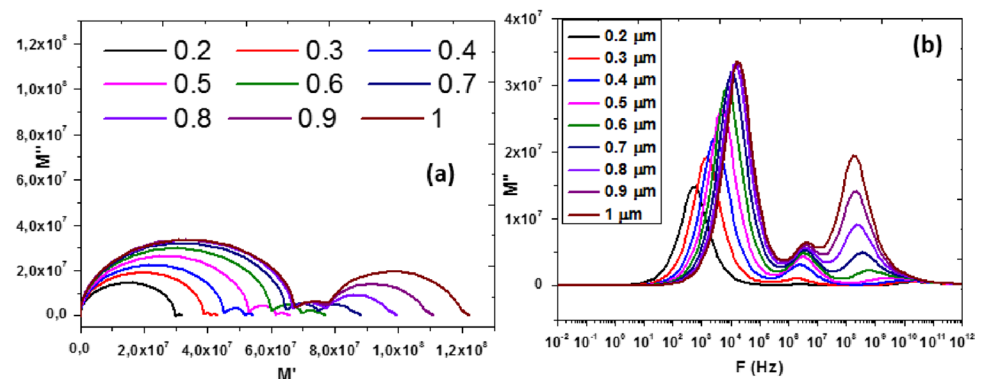
dynamic behavior of charge carriers due to the influence of layer thickness on diverse charge transport processes within the perovskite layer.

In Fig. 7b, the imaginary part (M″) versus frequency at each thickness showed the presence of three clearly defined relaxation processes, where their maxima become more apparent. These processes correlate with the semicircles observed in Fig. 7a, reinforcing the concept of multiple charge transport mechanisms. Furthermore, this representation with the imaginary part of impedance (M″) highlights the existence of two more relaxation processes and the coherence between these two processes of charge carrier dynamics. The identification of three consistent relaxation processes in both figures serves to affirm the intricate and multifaceted nature of charge transport within the perovskite solar cell. This frequency-dependent analysis offers an intricate perspective on the temporal behavior of charge carriers, illuminating the intricate interplay among various processes that contribute to the overall impedance response. The affirmation, as highlighted by the three consistent relaxation processes, echoes similar findings reported in previous studies investigating charge transport dynamics within the perovskite layer [29].

Figure 8a, b illustrate the comparison between the imaginary part of impedance (Z″) and the imaginary part of modulus (M″), yielding important insights into the dynamic processes governing the device's performance. Indeed, the identification of only a single relaxation process in Z″ at low frequency suggests a slow charge transport mechanism within the perovskite material. This could be associated with ion diffusion or charge carrier migration, emphasizing a primary relaxation event that significantly influences the electrical behavior of the solar cell at lower frequencies. The singular peak in Z″ suggests a distinct and pronounced response, providing clarity on the primary factor affecting the two other maxima, which are hidden in this frequency range.

On the other hand, the observation of three relaxation processes in the imaginary part of the modulus (M″) could highlight its very useful investigation. The low-frequency peak aligns with the slow relaxation process identified in Z″, reflecting similar ion migration phenomena. The appearance of medium and higher frequency peaks in M″ indicates the presence of additional dynamic events, possibly associated with recombination processes and charge transfer reactions. This multifaceted response in M″ suggests that the solar cell experiences distinct processes at different frequency regimes, providing a comprehensive view of the electrochemical and charge transport dynamics within the device. The three peaks in M″ collectively emphasize the significance of multiple relaxation events at varying rates, underscoring the complexity of the interactions contributing to the overall electrical performance of the perovskite solar cell across different frequency domains.
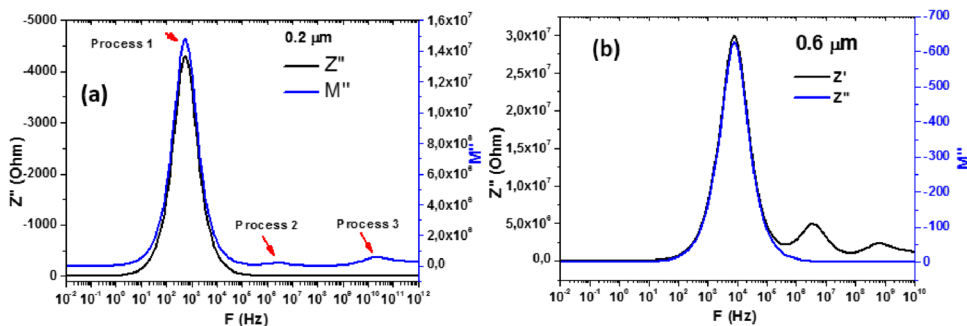
Analysis of the complex impedance (Z*) at different series (R_s) and shunt (R_{sh}) resistances

Figure 9a–c shows the impedance spectra in Nyquist and Bode plots for the solar cell perovskite at different series resistances (Rs). From Fig. 9a, it can be seen that the diameters of the semicircle do not change as the series resistance (Rs) increases from 0 up to 10 Ohm cm^2. However, with a close inspection, the increases in the series resistance (Rs) occur mainly at high frequencies from the intercept with the Z′ axis, as shown in the inset.

From Fig. 9b, it can also be seen that the maxima in the evolution of the imaginary part (Z″) versus frequency do not change as the series resistance (Rs) increases from 0 up to 10 Ω cm^2. This behavior correlates very well with the absence of a change in the diameters of the semicircles as shown in Fig. 9a. The absence of a significant change in the imaginary part of impedance (Z″) with variations in series resistance suggests that the charge carrier dynamics responsible for the imaginary component are less affected by the increase in series resistance.

However, it can be seen from Fig. 9c that there is a more pronounced shift in the real part (Z′), indicating a substantial impact in the high frequency regimes. This is illustrated by the significant change for Rs = 0, where there are two successive changes in the slope of the real part (Z′). This behavior implies that the series resistance is influencing

Fig. 8 **a**, **b** Superposition of the imaginary part (Z″) and (M″) of complex impedance and modulus at 0.2 μm and 0.6 μm of the perovskite layer thicknesses

**Fig. 9** Impedance spectra **a** Nyquist plot and **b**, **c** Bode plots solar cell perovskite at different series resistance (Rs)
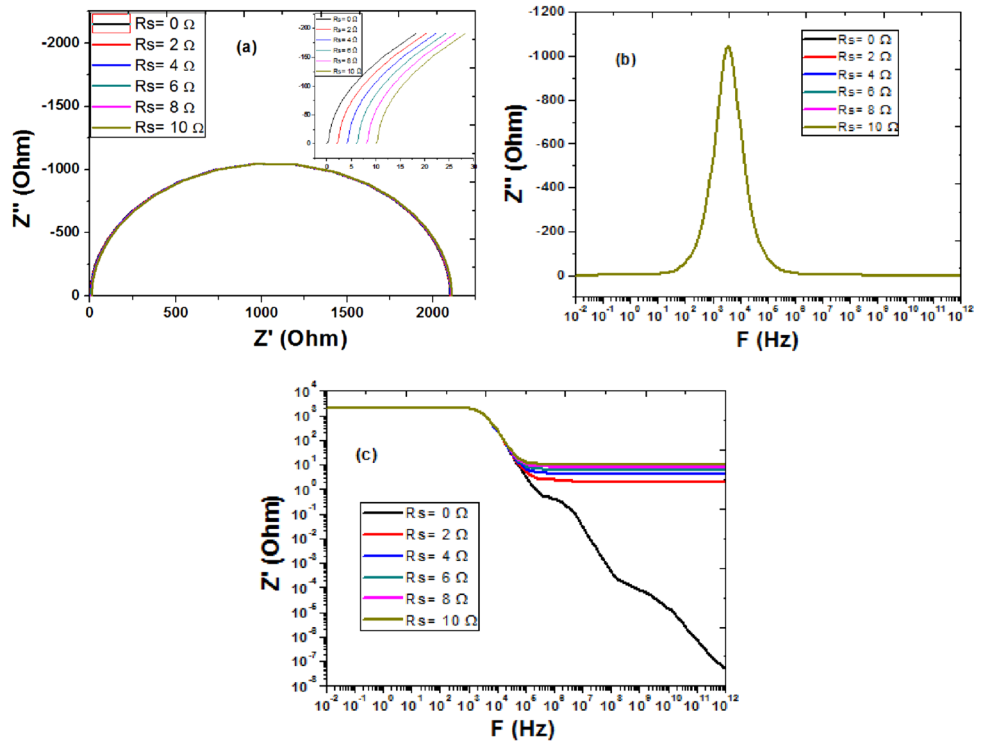
both processes for the dynamics of charge transport and recombination processes at medium and higher frequencies within the solar cell. These results provide crucial insights into the impact of series resistance on the impedance spectra of a perovskite solar cell.

Figure 10a–c shows the impedance spectra in Nyquist and Bode plots for a solar cell perovskite at different shunt resistances (Rsh) ranging from 200 up to 10^6 Ohm cm^2. In Fig. 10a, the Nyquist plot illustrates the impact of varying shunt resistance on the impedance spectra of a perovskite

Fig. 10 Impedance spectra **a** Nyquist plot and **b–d** bode plots of solar cell perovskite at different shunt resistance (Rsh)
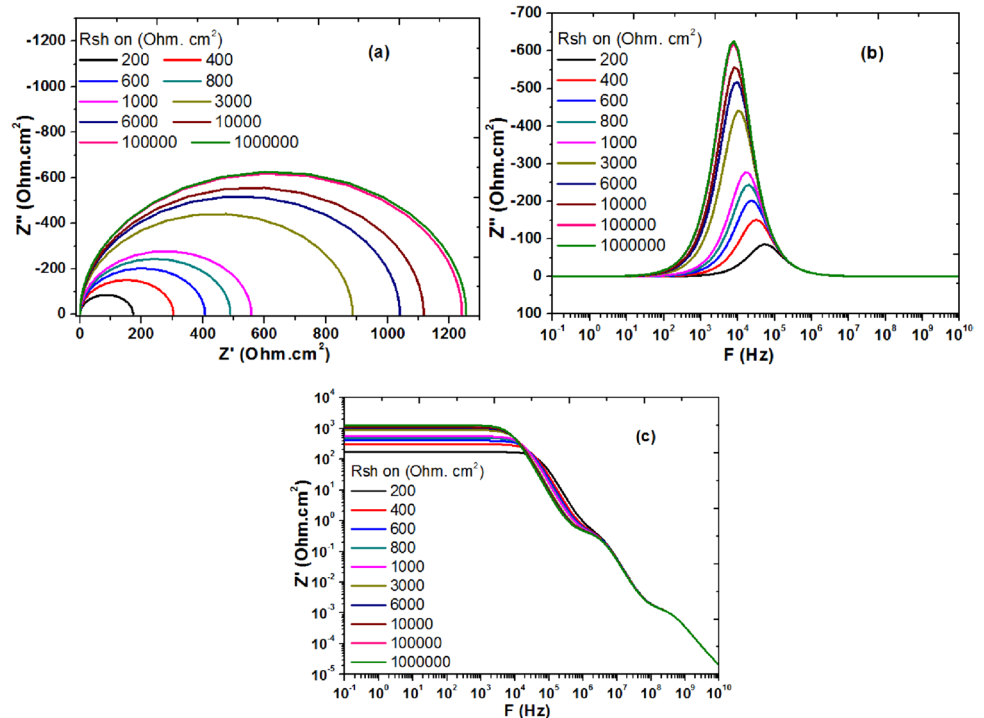
solar cell. As the shunt resistance increases, a noticeable change is observed specifically in the diameters of the semicircles. The increase in shunt resistance correlates with the increase of the diameters of these semicircles, suggesting alterations in the charge transfer processes within the solar cell, particularly at low frequencies.

Figure 10b provides further insight into the effect of shunt resistance on the imaginary part of impedance (Z″). The relaxation process, initially located at a specific frequency, undergoes a shift towards lower frequencies as the shunt resistance increases. This shift emphasizes the sensitivity of the ionic migration processes within the solar cell to changes in shunt resistance, indicating a modification in the characteristic timescales of these low-frequency phenomena.

Figure 10c reveals that the real part of impedance (Z′) is also affected by the change in shunt resistance, particularly at low frequencies. This observation implies that the alterations induced by variations in shunt resistance extend beyond the imaginary part of impedance, influencing the charge transfer dynamics at lower frequencies.

Analysis of the complex modulus (M*) at different series (Rs) and shunt (Rsh) resistance

In Fig. 11a, the use of the modulus function in the Nyquist diagram provides a comprehensive view of the impact of the series (Rs) resistance on the medium and high frequency processes. However, the diameter of the semicircle at the low frequency process did not show any change. For (Rs = 0), the three processes can be clearly observed, whereas from (Rs = 2), the medium and high frequency processes disappear.

Figure 11b in the Bode diagrams further supports and illustrates the behavior observed in the Nyquist plot (Fig. 11a). For (Rs = 0), the maxima for the three processes can be clearly observed, whereas from (Rs = 2), the maxima for the medium and high frequency processes are hidden.

This analysis reveals the pronounced effect of the series resistance (Rs) on the recombination and diffusion processes located at medium and higher frequencies. This attenuation indicates that the series resistance hinders the charge transfer and recombination events occurring at medium and higher frequencies. Figure 12a, b shows the modulus spectra of the solar cell perovskite at different shunt resistances (Rsh). As observed in Fig. 12a, the Nyquist diagram illustrates the effect of the shunt resistance (Rsh) resulting in the change of the diameters of the semicircles at low and medium frequencies. In contrast, the diameter of the semicircle at high frequency does not show any change.

Figure 12b represents the Bode diagrams, which provide a complementary view of the shunt resistance impact from the evolution of the imaginary part (M″) versus frequency. The Bode plots clearly show that the shunt resistance (Rsh) influences both processes at low and medium frequencies, corroborating the conclusion that the ionic migration and recombination processes are the

Fig. 11 Modulus spectra **a** Nyquist plot and **b** bode plots of solar cell perovskite at different series resistance (Rs)
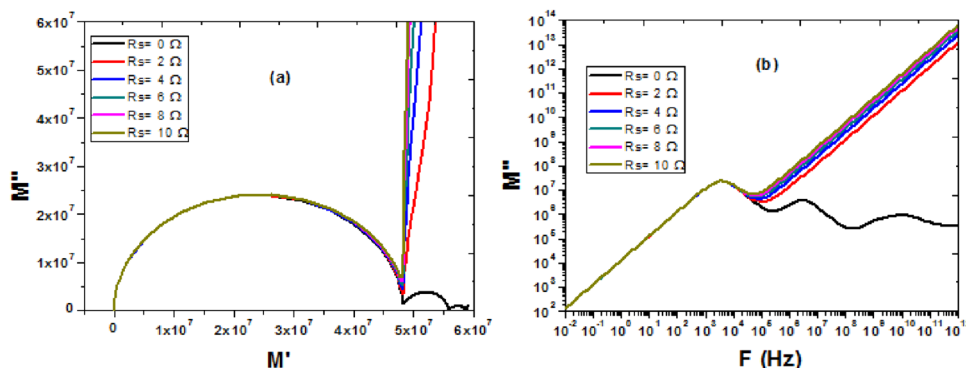
Fig. 12 Impedance spectra **a** Nyquist plot and **b** Bode plots of solar cell perovskite at different shunt resistance (Rsh)
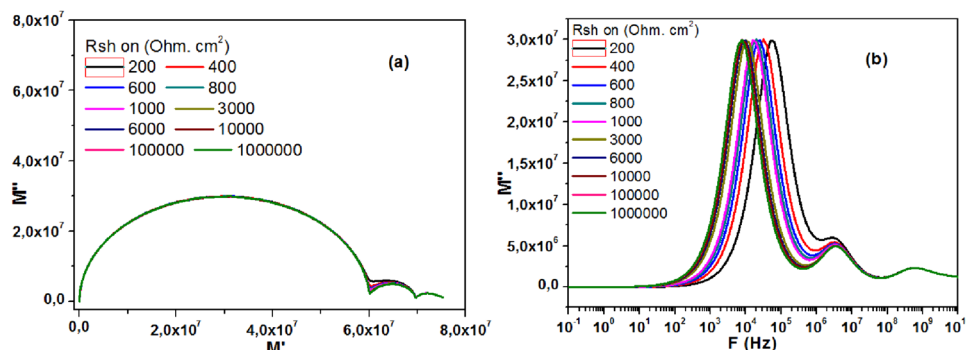
primary physical phenomena affected by changes in shunt resistance (Rsh). However, the process of diffusion at high frequency was not affected.

Theoretical considerations for modeling complex impedance (Z*) and modulus (M*) spectra

Various equivalent circuit models were used for solar cell analysis, including the Garcia-Belmonte series model [30], which lead to investigate the diffusion-recombination mechanisms, and the model proposed by Varun Srivastava et al. [31], featuring three interconnected blocks and a series resistance (Rs) accounting for cables and contacts. In our investigation the analysis showed that the evolution M″ versus frequency reveled the existence of three very well clears maximum a low and medium as well as at high frequency. In addition the observed peaks of Z″ and versus frequency M″ located at low-frequency occurs at the same frequency suggesting that are representing the same relaxation mechanism while the other process could be hidden. Therefore; the equivalent circuit shown in Fig. 13 was used to investigate the impedance (Z*) as well the modulus (M*). This equivalent circuit include a resistance (Rs) in series with three blocks composed with resistance in parallel with constant phase element: (R_1//CPE_1); (R_2//CPE_2) and (R_3//CPE_3. Each block could describe a distinct physical phenomenon in solar cell devices.
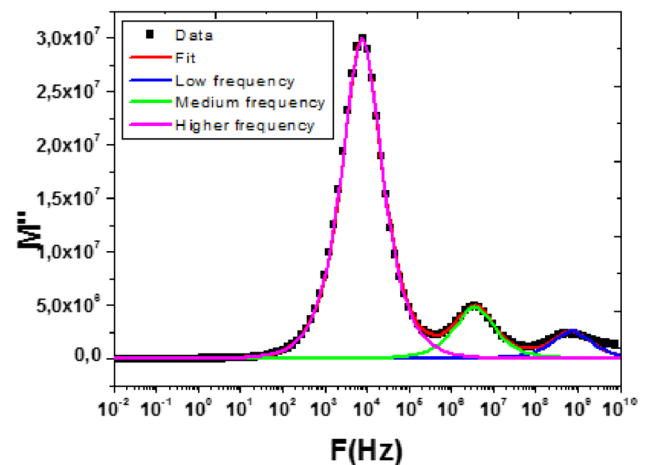
In Fig. 14, the evolution of the imaginary part (M″) versus frequency for (0.6 μm) thicknesses of the perovskite layer is selected as an example to illustrate the fitting with the above equivalent circuit. It can be seen that a good fitting was obtained with this circuit to highlight all processes. Additionally, a deconvolution procedure was carried out to isolate the three processes at low, medium, and high frequencies, as well as to validate the above equivalent circuit.

The deconvolution procedure was carried out to isolate the three processes at low, medium, and high frequencies, as well as to validate the above equivalent circuit. This led us to further investigate this validity from a theoretical point of view.

The complex impedance of the constant phase element, (CPE-T, p), is given as:
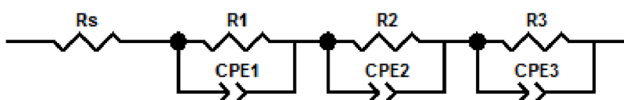
Fig. 13 Equivalent electrical circuit to fit and to analysis the complex impedance (Z*) and modulus (M*) spectrum

Fig. 14 Fit and de-convolution of process in the imaginary par (M″) versus frequency (M″) of solar cell perovskite at 0.6 μm

$$Z_{CPE} = \frac{1}{T(j\omega)^p} \tag{1}$$

where T is the pseudo-capacitance; ω is the angular frequency; $j^2 = -1$ is the imaginary number, and α is the CPE exponent. For $p = 1$, CPE is a pure capacitor (T = C); for p = 0, CPE is a pure resistance (T = 1/R); and for p = − 1, CPE is an inductor (T = 1/L).

The global complex impedance (Z*) of the above circuit can be written as the summation of Rs and the complex impedance (Z*) of each block.

$$Z^*(\omega) = R_s + \frac{R_1}{1+(j\omega\tau_1)^{P1}} + \frac{R_2}{1+(j\omega\tau_2)^{P2}} + \frac{R_3}{1+(j\omega\tau_3)^{P3}} \tag{2}$$

where $\tau_1 = (R_1C_1)^{1/p1}; \tau_2 = (R_2T_2)^{1/p2}, \tau_3 = (R_3T_3)^{1/p3}$.

From the fit with the above equivalent circuit, the values of the exponents P1, P2, and P3 are found to be close to 1. In this case, the CPE is a pure capacitance (T = C), and the Cole–Cole relaxation becomes equivalent to the Debye relaxation type. It's worth noting that this latter relaxation involves only a single relaxation time (τ), whereas for experimental measurements, the exponents P1, P2, and P3 are found to be less than 1 due to the distribution of the relaxation time (τ). Therefore, the total complex impedance of the above circuit is reduced as follows:

$$Z^*(\omega) = R_s + \frac{R_1}{1+(j\omega\tau_1)} + \frac{R_2}{1+(j\omega\tau_2)} + \frac{R_3}{1+(j\omega\tau_3)} \tag{3}$$

where $\tau_1 = R_1C_1; \tau_2 = R_2C_2$ and $\tau_3 = R_3C_3$.

The expressions for the angular frequencies (ω_{1max}); (ω_{2max}) and (ω_{3max}) can also be derived from the derivative of the imaginary part (M″) with respect to angular frequency

(ω). This results in obtaining the same specific value (ω_{max}) corresponding to each maximum observed in the evolution of the imaginary part (M'').

$$\omega_{1\,max} = 2\pi f_{1\,max} = \frac{1}{\tau_1} = \frac{1}{R_1 C_1}, \quad \omega_{2\,max} = 2\pi f_{2\,max} = \frac{1}{\tau_2} = \frac{1}{R_2 C_2}, \quad \omega_{3\,max} = 2\pi f_{3\,max} = \frac{1}{\tau_3} = \frac{1}{R_3 C_3}$$

Hence, the above expressions could explain why each maximum observed in the evolution of the imaginary part of both (Z'') and (M'') at both low and high frequencies occurs at the same specific frequency value (F_{max}).

Analysis of extracted parameters from the equivalent circuit

Effect of the perovskite thickness (L) on the relaxation times and efficiency

The observed trends in the relaxation processes and their correlation with solar cell parameters provide valuable insights into the overall performance of lead-free perovskite solar cells (PSCs). The evolutions of the time constants τ_1 and τ_2, as well as the efficiency η (%), at different perovskite thicknesses, are shown in Fig. 15a–c.

According to the characteristic time constants τ_1, τ_2, and τ_3, it can be seen that they are representative of a slow, fast, and even faster process. Additionally, it is well-known that perovskite solar cells exhibit mixed electronic-ionic conductivity [12]. In this case, it is expected that the three

relaxation processes could occur due to ionic migration, recombination, as well as the diffusion of charge carriers for electrons and holes. Therefore, the characteristic time constants (τ_1), (τ_2), and (τ_3) represent the relaxation time of the diffusion, recombination, and the ionic charge migrations processes, respectively.

Figure 8a show the effect of thickness on diffusion relaxation time and its correlation with efficiency in perovskite solar cells, it is a critical aspect of understanding and optimizing their performance. As the thickness of the perovskite layer increases, the diffusion relaxation time (τ) generally tends to increase as well. Initially, at lower thicknesses, the diffusion relaxation time may remain relatively stable or increase slowly. This is because thinner layers allow for faster diffusion of charge carriers due to shorter distances for carriers to travel. However, beyond 0.6 mm optimal thickness, the diffusion relaxation time may start to increase rapidly. This is often due to increased recombination rates and reduced carrier mobility in thicker layers, leading to slower diffusion of charge carriers. The specific relationship between thickness and diffusion relaxation time can vary depending on factors such as material properties, device architecture, and fabrication techniques.

Figure 15b show the effect of thickness on recombination relaxation time and its correlation with efficiency in perovskite solar cells, it is a critical aspect of understanding and optimizing their performance. The recombination processes represented by τ_2 play a crucial role in determining

Fig. 15 **a–c** Effect of thickness (L) on extracted parameters of equivalent electrical circuit
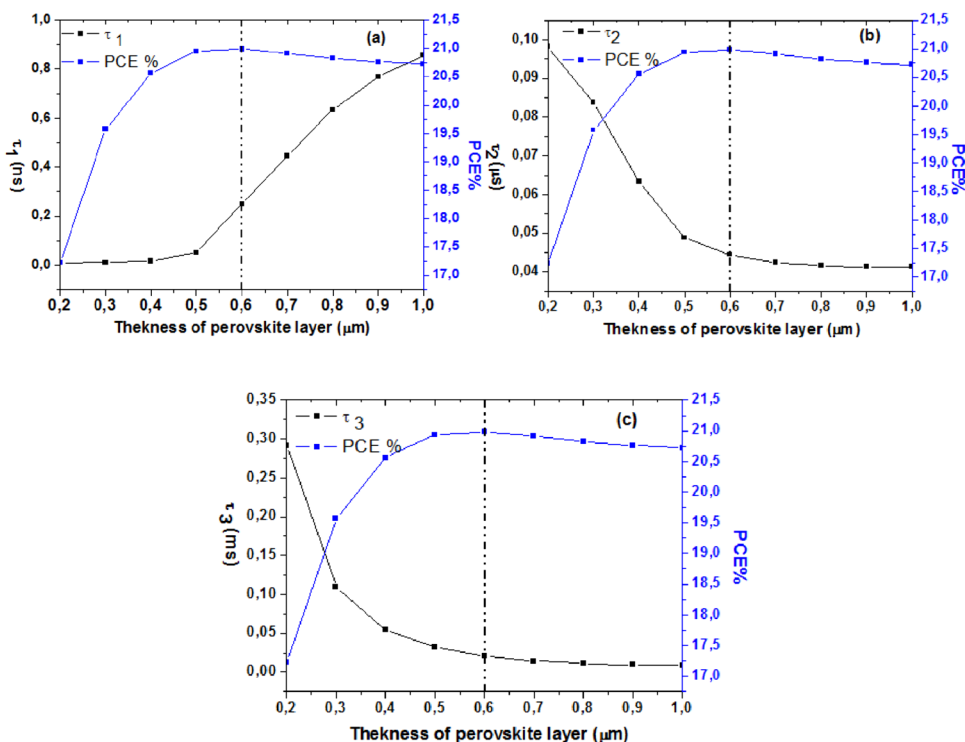
the efficiency of perovskite solar cells. A rapid decrease in τ_2 up to a thickness of 0.6 mm indicates a reduction in recombination time. This reduction is a positive factor for efficient charge collection within the solar cell. The observed rapid decline in τ_2 up to 0.6 mm aligns with the desired outcome of reducing recombination losses, which typically enhances the overall efficiency of the solar cell.

This reduction in recombination time corresponds to improved charge collection efficiency, as fewer charge carriers recombine before being collected. However, this reduction in recombination time also presents a trade-off, particularly in relation to the fill factor (FF) of the solar cell.

The fill factor, a key parameter representing the efficiency of charge collection and utilization within the solar cell, typically declines rapidly up to 0.6 mm. This decline in FF% suggests that while thicker perovskite layers may promote better charge collection, they can also lead to increased recombination losses, which negatively impact the fill factor. Therefore, there exists a delicate balance between optimizing charge collection efficiency through thicker perovskite layers and minimizing recombination losses to maintain a high fill factor.

Figure 15a show the effect of thickness on ionic transport relaxation time and its correlation with efficiency. The observed decrease in τ_3, which is associated with ionic transport, up to a thickness of 0.6 mm, suggests a notable improvement in the efficiency of charge transport within the perovskite layer. This reduction implies that thinner perovskite layers allow for more efficient movement of ionic charge carriers, such as ions, through the material. Improved

ionic transport is crucial for facilitating the movement of charge carriers within the solar cell, ultimately contributing to enhanced performance. Beyond a thickness of 0.6 mm, τ_3 stabilizes, indicating that an optimal thickness range has been reached for maximizing ionic conductivity within the perovskite layer. This stabilized τ_3 suggests that further reductions in thickness may not significantly enhance ionic transport and may even lead to diminishing returns in terms of performance improvement. Therefore, maintaining a thickness within this optimal range is crucial for achieving the highest possible PCE.

Impact of the shunt (R_{sh}) resistance on the efficiency

The impedance spectroscopy analysis of the solar cells, as discussed earlier, unveiled three distinct relaxation processes attributed to different frequency ranges: low frequency associated with ionic transport relaxation (τ_3), medium frequency linked to recombination processes (τ_2), and high frequency indicative of electronic transport (diffusion) (τ_1) within the perovskite layer.

Figure 16a–c, show the effect of shunt resistance (Rsh) on the diffusion relaxation time (τ_1), recombination relaxation time (τ_2), and ionic transport relaxation time (τ_3), along with their correlation with efficiency, is illustrated.

The observed trends indicate that all three relaxation times (τ_1, τ_2, and τ_3) increase with increasing shunt resistance (Rsh) until reaching a value of 10^4 Ω cm^2. Beyond this resistance threshold, all three relaxation times stabilize.

Fig. 16 a–c Effect of Rsh on extracted parameters of equivalent electrical circuit
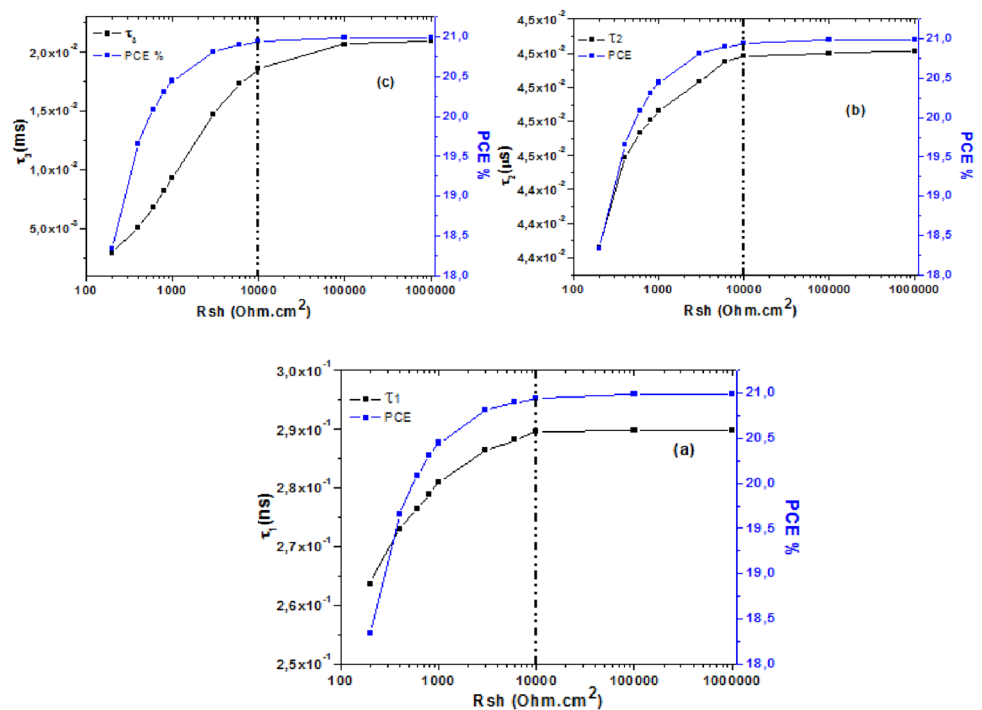
Interestingly, the trend in relaxation times correlates closely with the efficiency of our perovskite solar cell.

The increase in relaxation times with increasing shunt resistance suggests that higher shunt resistance hinders charge transport within the perovskite layer. This impediment results in longer relaxation times for all three processes, indicating slower charge carrier movement. However, once the shunt resistance exceeds $10^4 \, \Omega \, cm^2$, the relaxation times stabilize, indicating a saturation point where further increases in shunt resistance do not significantly affect charge transport dynamics within the perovskite layer.

The observed relationship between shunt resistance, relaxation times, and efficiency underscores the importance of optimizing charge transport dynamics within the perovskite layer for maximizing the performance of perovskite solar cells. Understanding these dynamics can inform strategies for improving device efficiency and stability.

Conclusion

This study revealed that the analysis of complex impedance (Z*) combined with complex modulus (M*), using simultaneously Bode and Nyquist diagrams, can be considered the most appropriate approach to investigate the different processes involved in lead-free perovskite solar cells (PSCs). Exploring complex impedance (Z*) and modulus (M*) over a wide frequency range allowed for the identification of diffusion, recombination, and ionic transport processes. Additionally, theoretical considerations coupled with deconvolution procedures were instrumental in confirming the existence of these different processes. A strong correlation was observed between the time constants for each process and the power conversion efficiency (PCE).

This comprehensive analysis of lead-free PSCs reveals intricate dynamics governing their performance. The optimal thickness (L) was identified as a critical factor influencing PCE. The observed trends in ionic transport, recombination processes, and electronic diffusion highlight the delicate balance required to maximize charge transport while minimizing recombination losses. Beyond the optimal thickness of 0.6 μm, the interplay of electronic transport processes (τ_1) with shunt resistance (Rsh) becomes crucial.

These findings underscore the importance of selecting the appropriate thickness for the absorbing material and recognizing the impact of series (Rs) and shunt (Rsh) resistance in enhancing the efficiency of lead-free PSCs. Further research is underway to investigate these lead-free PSCs under different bias voltages (Vbias), illumination conditions, and temperatures.

Declarations

References

1. Singh, K.A.S., Mohammed, M.K., Shalan, A.E.: Effect of 2D perovskite layer and multivalent defect on the performance of 3D/2D bilayered perovskite solar cells through computational simulation studies. Sol. Energy **223**, 193–201 (2021)

2. Al-Mousoi, A., Mehde, M., Al-Gebori, A.: Annealing temperature effects on the performance of the perovskite solar cells. IOP Conf. Ser. Mater. Sci. Eng. **757**, 012039 (2020)

3. Mohammed, M.K., Al-Mousoi, A.K.: Deposition of multilayer graphene (MLG) film on glass slide by fame synthesis technique. Optik **127**(20), 9848–9852 (2016)

4. Correa-Baena, J.-P., Saliba, M., Buonassisi, T., Grätzel, M., Abate, A., Tress, W., Hagfeldt, A.J.S.: Promises and challenges of perovskite solar cells. Science **358**(6364), 739–744 (2017)

5. Kadhim, M.J., Mohammed, M.K.: Fabrication of efficient triple-cation perovskite solar cells employing ethyl acetate as an environmental-friendly solvent additive. Mater. Res. Bull. **158**, 112047 (2022)

6. Davenport, P., Ma, Z., Schirck, J., Nation, W., Morris, A., Wang, X., Lambert, M.: Characterization of solid particle candidates for application in thermal energy storage and concentrating solar power systems. Sol. Energy **262**, 111908 (2023)

7. Lu, X., Mu, C., Liu, Y., Wu, L., Tong, Z., Huang, K.: Recent advances in solar-driven interfacial evaporation coupling systems:

energy conversion, water purification, and seawater resource extraction. Nano Energy 109180 (2023)

8. Aquilas, N.A., Atemnkeng, J.T.: Climate-related development finance and renewable energy consumption in greenhouse gas emissions reduction in the Congo basin. Energy Strategy Rev. **44**, 100971 (2022)

9. Huo, J., Peng, C.: Depletion of natural resources and environmental quality: prospects of energy use, energy imports, and economic growth hindrances. Resour. Policy **86**, 104049 (2023)

10. Khan, Y., Hassan, T.: Promoting sustainable development: Evaluating the influence of natural resources, high-tech export and corruption on CO_2 emissions in developing economies. Resour. Policy **88**, 104511 (2024)

11. Kareem, S.H., Elewi, M.H., Naji, A.M., Ahmed, D.S., Mohammed, M.K.: Efficient and stable pure a-phase FAPbI3 perovskite solar cells with a dual engineering strategy: additive and dimensional engineering approaches. Chem. Eng. J. **13**, 136469 (2022)

12. Mohammed, M.K., Jabir, M.S., Abdulzahraa, H.G., Mohammed, S.H., Al-Azzawi, W.K., Ahmed, D.S., Singh, S., Kumar, A., Asaithambi, S., Shekargoftar, M.: Introduction of cadmium chloride additive to improve the performance and stability of perovskite solar cells. RSC Adv. **12**(32), 20461–20470 (2022)

13. Al-Mousoi, A.K., Mohammed, M.K.: Engineered surface properties of MAPI using different antisolvents for hole transport layer-free perovskite solar cell (HTL-free PSC). J. Sol-Gel Sci. Technol. **96**(3), 659–668 (2020)

14. Kojima, A., Teshima, K., Shirai, Y., Miyasaka, T.: Organometal halide perovskites as visible-light sensitizers for photovoltaic cells. J. Am. Chem. Soc. **131**(17), 6050–6051 (2009)

15. Min, H., Lee, D.Y., Kim, J., Kim, G., Lee, K.S., Kim, J., Paik, M.J., Kim, Y.K., Kim, K.S., Kim, M.G.J.N.: Perovskite solar cells with atomically coherent interlayers on SnO2 electrodes. Nature **598**(7881), 444–450 (2021)

16. Cao, J., Yan, F.J.E., Science, E.: Recent progress in tinbased perovskite solar cells. Energy Environ. Sci. **14**(3), 1286–1325 (2021)

17. Schileo, G., Grancini, G.: Lead or no lead? Availability, toxicity, sustainability and environmental impact of leadfree perovskite solar cells. J. Mater. Chem. C **9**(1), 67–76 (2021)

18. Hoefer, S.F., Trimmel, G., Rath, T.: Progress on lead-free metal halide perovskites for photovoltaic applications: a review. Chem. Mon. **148**(5), 795–826 (2017)

19. Shen, G., Dong, H., Yang, F., Ng, X.R., Li, X., Lin, F., Mu, C.: Application of an amphipathic molecule at the NiOx/perovskite interface for improving the efficiency and long-term stability of the inverted perovskite solar cells. J. Energy Chem. **78**, 454–462 (2023)

20. Rahman, M.S., Miah, S., Marma, M.S.W., Sabrina, T.: Simulation based investigation of inverted planar perovskite solar cell with all metal oxide inorganic transport layers. In: 2019 International Conference on Electrical, Computer and Communication Engineering (ECCE), IEEE, pp. 1–6 (2019)

21. Al-Mousoi, A.K., Mohammed, M.K., Pandey, R., Madan, J., Dastan, D., Ravi, G., Sakthivel, P.: Simulation and analysis of

22. Mortadi, A., El Hafidi, E., Monkade, M., El Moznine, R.: Investigating the influence of absorber layer thickness on the performance of perovskite solar cells: a combined simulation and impedance spectroscopy study. Mater. Sci. Energy Technol. **7**, 158–165 (2024)

23. Rahman, M.S., Miah, S., Marma, M.S.W., Sabrina, T.: Simulation based investigation of inverted planar perovskite solar cell with all metal oxide inorganic transport layers. In: 2019 International Conference on Electrical, Computer and Communication Engineering (ECCE), pp 1–6. IEEE (2019)

24. Şahin, G., Alma, M.H.: Study of the static characteristic IV and the electrical parameters corresponding to the shunt resistance Rsh and series resistance Rs per unit area of a solar cell with grain size. Chin. J. Phys. **62**, 395–404 (2019)

25. Amiri, O., Salavati-Niasari, M.: High efficiency dye-sensitized solar cells (9.3%) by using a new compact layer: decrease series resistance and increase shunt resistance. Mater. Lett. **160**, 24–27 (2015)

26. Khalili, S., Chenari, H., Orhan, Z., F, Yıldırım, S, Aydoğan,: Synthesis characterization of SnO_2 nanofibers (NFs) and application of high-performing photodetectors based on SnO2 NFs/n-Si heterostructure. Sens. Actuators A Phys. **342**, 113631 (2022)

27. Musiienko, A., Moravec, P., Grill, R., Praus, P., Vasylchenko, I., Pekarek, J., Ahmadi, M.: Deep levels, charge transport and mixed conductivity in organometallic halide perovskites. Energy Environ. Sci. **12**(4), 1413–1425 (2019)

28. Azpiroz, J.M., Mosconi, E., Bisquert, J., De Angelis, F.: Defect migration in methylammonium lead iodide and its role in perovskite solar cell operation. Energy Environ. Sci. **8**(7), 2118–2127 (2015)

29. Tailor, N.K., Senanayak, S.P., Abdi-Jalebi, M., Satapathi, S.: Low-frequency carrier kinetics in triple cationperovskite solar cells probed by impedance and modulus spectroscopy. Electrochim. Acta **386**, 138430 (2021)

30. Garcia-Belmonte, G., Munar, A., Barea, E.M., Bisquert, J., Ugarte, I., Pacios, R.: Charge carrier mobility and lifetime of organic bulk heterojunctions analyzed by impedance spectroscopy. Org. Electron. **9**(5), 847–851 (2008)

31. Srivastava, V., Alexander, A., Anitha, B., Namboothiry, M.A.: Impedance spectroscopy study of defect/ion mediated electric field and its effect on the photovoltaic performance of perovskite solar cells based on different active layers. Sol. Energy Mater. Sol. Cells **237**, 111548 (2022)